Article

Electrochemical Study of a Reconstituted Photosynthetic Electron-Transfer Chain

Vincent Fourmond, Bernard Lagoutte, Pierre Stif, Winfried Leibl, and Christophe Demaille

J. Am. Chem. Soc., **2007**, 129 (29), 9201-9209• DOI: 10.1021/ja0714787 • Publication Date (Web): 28 June 2007

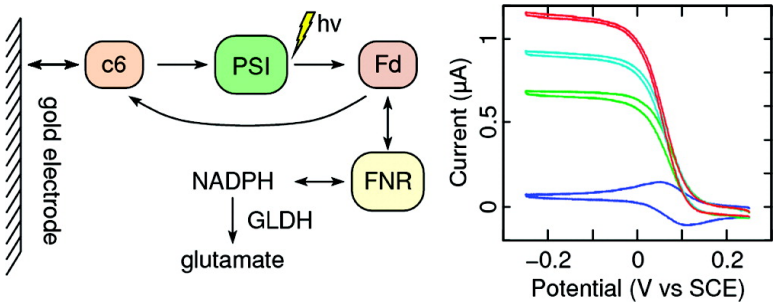

More About This Article

Additional resources and features associated with this article are available within the HTML version:

- Supporting Information
- Links to the 2 articles that cite this article, as of the time of this article download
- Access to high resolution figures
- Links to articles and content related to this article
- Copyright permission to reproduce figures and/or text from this article

View the Full Text HTML

J|A|C|S
ARTICLES
Published on Web 06/28/2007

Electrochemical Study of a Reconstituted Photosynthetic Electron-Transfer Chain

Vincent Fourmond,[‡] Bernard Lagoutte,[‡] Pierre Sétif,[‡] Winfried Leibl,*[,‡] and Christophe Demaille*[,†]

Contribution from the CEA, Institut de Biologie et de Technologies de Saclay, URA 2096, Gif sur Yvette, F-91191, France, and Laboratoire d'Électrochimie Moléculaire, UMR du CNRS N°7591, Université Paris VII—Denis Diderot, 75251 Paris cedex 05, France

Received March 2, 2007; E-mail: winfried.leibl@cea.fr; christophe.demaille@paris7.jussieu.fr

Abstract: A multi-enzyme electron-transfer chain involving solubilized photosystem I (PSI) as photocatalytic unit, cytochrome c_6 and ferredoxin as electron carriers and ferredoxin/NADPH oxidoreductase (FNR) as electron acceptor was reconstituted in an electrochemical cell and studied by cyclic voltammetry. The working gold electrodes were modified to react selectively with cytochrome c_6. Quantitative analysis of the photocatalytic current under continuous illumination allowed the determination of the values k_{on} and k_{off} for the ferredoxin/PSI interaction. An efficient recycling system for NADPH was established, and the dissociation constant of the oxidized ferredoxin/semiquinone FNR complex was extracted by modeling the catalytic efficiency of the chain as a function of ferredoxin concentration. The value determined hereby is consistent with a shift of −50 to −100 mV of the reduction potential of ferredoxin when complexed with FNR.

Introduction

Metabolic pathways in biological systems are complex interconnected networks of proteins and enzymes interacting in an optimized way. The reaction sequences typically involve transfer of electrons and protons to or from specific catalytic sites where bond-forming or bond-breaking reactions occur. Probably the most studied examples are the electron-transfer chains of respiration and photosynthesis. Especially photosynthesis has become an important model system because of the intrinsic property that the reaction sequences can easily be initiated by short flashes of light thus allowing kinetic studies with high time resolution.

Natural photosynthesis is the process in which autotrophic organisms use the energy of sunlight to create reducing equivalents which drive carbon assimilation. In plants, green algae and cyanobacteria, electrons extracted from water by photosystem II are channeled along a membrane-bound electron-transfer chain toward the oxidizing side of photosystem I (PSI). The structure of cyanobacterial PSI reveals a membrane protein complex assembled from 12 subunits and carrying 127 pigments and cofactors.[1] Upon illumination, excitation of the primary donor P700 triggers a sequence of fast internal electron-transfer reactions where an electron is displaced from P700 onto one of the internal electron acceptors F_A or F_B, which are 4Fe-4S clusters. In this way a charge separation state ($P700^+ F_{AB}^-$) is created within less than one microsecond.[2] PSI interacts with small soluble redox active proteins at both the donor and the acceptor side. The oxidized primary donor $P700^+$ oxidizes reduced plastocyanin or cytochrome c_6 ($E_m = +321$ mV vs NHE[3]) on the lumenal side of the membrane whereas F_B reduces ferredoxin (Fd) on the stromal side of the membrane. Ferredoxin as low-potential electron carrier ($E_m \approx -420$ mV vs NHE[4]) plays a central role as the entry point of electrons for a series of redox metabolic cycles, such as nitrogen and sulfur assimilation. Recently, the interaction of Fd with hydrogenases, which catalyze the reversible reduction of protons to dihydrogen in some photosynthetic microorganisms, has become a topic of special interest with respect to the optimization of metabolic pathways of genetically engineered organisms designed for H_2 production.[5,6] However, the main partner of Fd in the bioenergetic pathway, competing with hydrogenase for low potential electrons from PSI, is the enzyme ferredoxin-$NADP^+$-reductase (FNR). FNR is a well characterized flavoprotein of 34 kDa that oxidizes two equivalents of reduced Fd to produce one equivalent of NADPH from $NADP^+$. NADPH is the source of reducing equivalents for carbon assimilation in the Calvin cycle. With regard to the optimization of electron flow toward hydrogenase it is therefore of considerable interest to study the electron-transfer chain on the reducing side of PSI with the aim to determine the factors which govern the interaction between PSI and Fd as well as between Fd and FNR. Of course, such a study will have to be complemented by an analogous study of

[‡] CEA.
[†] Université Paris VII.

(1) Jordan, P.; Fromme, P.; Witt, H. T.; Klukas, O.; Saenger, W.; Krauss, N. *Nature* **2001**, *411*, 909−917.
(2) Brettel, K.; Leibl, W. *Biochim. Biophys. Acta* **2001**, *1507*, 100−114.
(3) Proux-Delrouyre, V.; Demaille, C.; Leibl, W.; Sétif, P.; Bottin, H.; Bourdillon, C. *J. Am. Chem. Soc.* **2003**, *125*, 13686−13692.
(4) Batie, C.; Kamin, H. *J. Biol. Chem.* **1986**, *261*, 11214−11223.
(5) Cournac, L.; Mus, F.; Bernard, L.; Guedeney, G.; Vignais, P.; Peltier, G. *Int. J. Hydrogen Energy* **2002**, *27*, 1229−1237.
(6) Fouchard, S.; Hemschemeier, A.; Caruana, A.; Pruvost, J.; Legrand, J.; Happe, T.; Peltier, G.; Cournac, L. *Appl. Environ. Microbiol.* **2005**, *71*, 6199−6205.

the interaction between Fd and hydrogenase once the purification of this enzyme in an active form is established.

During the last decades, different spectroscopic techniques have been successfully applied to characterize transient intermediates in enzymes thus revealing structure−function relationships and the principles governing the interactions between the reaction partners.[7] With few exceptions such studies are made on isolated complexes and their direct partners. Certainly, this approach is very efficient to understand a given molecular mechanism of a subensemble, but it is also of considerable interest to investigate as far as possible the complete reaction chain to approach the physiological relevant conditions.

Electrochemical methods provide an efficient alternative to spectroscopy to probe the kinetics of photosynthetic electron-transfer.[3] Kinetic measurements based on the coupling between a heterogeneous reaction at an electrode and a catalytic reaction have been used for over half a century.[8] On the basis of the work from Nicholson and Shain[9,10] and Savéant and Vianello,[11] literature now offers several theoretical frameworks for electrocatalysis which allow us to obtain rate constants from catalytic currents measured for homogeneous catalysis[12,13] or direct electron transfer.[14] These techniques have proved useful for the elucidation of the functional mechanisms for numerous enzymes, including hydrogenases,[15,16] glucose oxidase,[13] fumarate reductase,[17] horseradish peroxidase,[18] FNR,[19,20] and cytochrome $P450_{cam}$.[21] As a special case, photocatalytic systems offer the advantage over other catalytic systems that catalysis can be turned on and off with the actinic light. Several groups have attempted electrochemical studies of photosystem I, taking advantage of its tendency to adsorb onto hydroxyl-covered surfaces[22−24] or embedding it into a supported lipid bilayer on an electrode.[25] Though groups reported promising conditions for direct electrochemistry of photosystem I,[23,25] none provided new insights into the functional aspects of photosystem I or the interaction with its natural redox partners.

In this work we reconstituted "ex-vivo", inside an electrochemical cell, a complete photosynthetic electron-transfer chain involving PSI, its direct electron donors and acceptors cyt c_6[26] and Fd, respectively, as well as FNR and its substrate $NADP^+$. As all proteins were solubilized, conditions of the study were very close to those used for spectroscopic measurements.[27−30] The catalytic current of the system was studied under continuous illumination conditions with cyclic voltammetry. Once sufficient NADPH recycling conditions were established, variation of the relative concentration of partners of the chain permitted to chose different reaction steps to be rate limiting. The electrocatalytic data obtained were analyzed within an adapted theoretical framework, and relevant rate constants and interaction parameters were extracted.

Experimental Section

Materials. 3-Mercapto-1-propanol, β-nicotinamide adenine nucleotide phosphate ($NADP^+$), glutamate dehydrogenase (EC 1.4.1.4) from *Proteus* (GLDH), α-ketoglutarate (α-KG), titanium(III) chloride, trisodium citrate, and β-dodecyl maltoside (β-DM) were purchased from Sigma-Aldrich (St Quentin Fallavier, France). Gold (purity 99.999%) was purchased from Platecxis (Noisy le Sec, France). Organic solvents were HPLC grade. Silver glue was from Epotecny (Levallois-Perret, France). Water with a typical resistivity of 18.2 MΩ was obtained from a Milli-Q purification system (Millipore, Les Ulis, France). Sulfuric acid was 95% pure. Titanium(III) citrate was made as described in ref 31, note 3.

Depending on the needs, two buffers were used: the "partial" buffer contained 20 mM tricine pH 8, 25 mM $(NH_4)_2SO_4$, 15 mM α-KG and 5 mM $MgSO_4$. The "complete" buffer contained in addition 2 mM $NADP^+$ and 0.03% β-DM, the latter being necessary to prevent adsorption of PSI I on hydroxyl-covered electrodes.[24]

Protein Purification. Cytochrome c_6 from *Thermosynechococcus elongatus* was purified to homogeneity from a batch of the prepurified protein (gift from Dr A. Boussac) by a gel permeation chromatography on a superdex 75 column (Pharmacia). The starting batch resulted from a classical series of steps: ammonium sulfate precipitation, anion exchange, and hydrophobic chromatographies.[3] Fully oxidized cyt c_6 was obtained in the presence of an excess of potassium ferricyanide. Binding of the oxidized cyt c_6 on phenyl sepharose at 50% saturation of ammonium sulfate allowed a fast and complete desalting, followed by elution in MES buffer, 20 mM, pH 6.5. Concentrations of the stock solutions were measured spectrophotometrically using an extinction coefficient of 25.5 $mM^{-1}\cdot cm^{-1}$ at 553 nm for the reduced form and of 11.5 at 526 nm for the oxidized form.

The PSI reaction centers, Fd and FNR, were isolated from *Synechocystis* sp PCC 6803. The monomeric form of PSI was purified following the original method of Rögner et al.[32] A modification of the anion exchange was introduced, ammonium sulfate replacing magnesium chloride as the eluting salt. Stock solutions of PSI were usually at a concentration of 23 μM P700. The plasmid (pET22b) for the expression of an intermediate form of FNR (75 aa deletion from the N-terminal) was a gift from Dr. J. van Thor.[33] The Fd gene was PCR amplified and cloned in an expression vector of the pET series.[34] Both proteins were overexpressed in *E. coli* and purified by successive steps of ammonium sulfate precipitation, anion exchange, and hydrophobic

(7) Carrillo, N.; Ceccarelli, E. A. *Eur. J. Biochem.* **2003**, *270*, 1900−1915.
(8) Savéant, J. M.; Vianello, E. *Adv. Polarogr., Proc. Int. Congr. 2nd* **1960**, *1*, 367−374.
(9) Nicholson, R. S.; Shain, I. *Anal. Chem.* **1964**, *36*, 706−723.
(10) Nicholson, R. S.; Shain, I. *Anal. Chem.* **1965**, *37*, 178−190.
(11) Savéant, J. M.; Vianello, E. *Electrochim. Acta* **1965**, *10*, 905−920.
(12) Cass, A. E. G.; Davis, G.; Francis, G. D.; Hill, H. A. O.; Aston, W. J.; Higgins, I. J.; Plotkin, E. V.; Scott, L. D. L.; Turner, A. P. F. *Anal. Chem.* **1984**, *56*, 667−671.
(13) Bourdillon, C.; Demaille, C.; Moiroux, J.; Savéant, J. M. *J. Am. Chem. Soc.* **1993**, *115*, 1−10.
(14) Heering, H. A.; Hirst, J.; Armstrong, F. A. *J. Phys. Chem. B* **1998**, *102*, 6889−6902.
(15) Léger, C.; Jones, A. K.; Roseboom, W.; Albracht, S. P. J.; Armstrong, F. A. *Biochemistry* **2002**, *41*, 15736−15746.
(16) De Lacey, A. L.; Moiroux, J.; Bourdillon, C. *Eur. J. Biochem.* **2000**, *267*, 6560−6570.
(17) Léger, C.; Heffron, K.; Pershad, H.; Maklashina, E.; Luna-Chavez, C.; Cecchini, G.; Ackrell, B.; Armstrong, F. *Biochemistry* **2001**, *40*, 11234−11245.
(18) Dequaire, M.; Limoges, B.; Moiroux, J.; Savéant, J.-M. *J. Am. Chem. Soc.* **2002**, *124*, 240−253.
(19) Madoz, J.; Fernandez-Recio, J.; Gomez-Moreno, C.; Fernandez, V. M. *Bioelectrochem. Bioenerg.* **1998**, *47*, 179−183.
(20) Akashi, T.; Matsumura, T.; Ideguchi, T.; Iwakiri, K.; Kawakatsu, T.; Taniguchi, I.; Hase, T. *J. Biol. Chem.* **1999**, *274*, 29399−405.
(21) Wirtz, M.; Klucik, J.; Rivera, M. *J. Am. Chem. Soc.* **2000**, *122*, 1047−1056.
(22) Kievit, O.; Brudvig, G. W. *J. Electroanal. Chem.* **2001**, *497*, 139−149.
(23) Ciobanu, M.; Kincaid, H. A.; Lo, V.; Dukes, A. D.; Kane Jennings, G.; Cliffel, D. E. *J. Electroanal. Chem.* **2007**, *599*, 72−78.
(24) Lee, I.; Lee, J. W.; Greenbaum, E. *Phys. Rev. Lett.* **1997**, *79*, 3294−3297.
(25) Munge, B.; Das, S. K.; Ilagan, R.; Pendon, Z.; Yang, J.; Frank, H. A.; Rusling, J. F. *J. Am. Chem. Soc.* **2003**, *125*, 12457−12463.
(26) Cyt c_6 was preferred over plastocyanin as it is easy to purify to homogeneity and has been already used in our previous work with photosystem I. Both molecules have very similar kinetics and efficiency for reduction of $P700^+$.
(27) Sétif, P. *Biochim. Biophys. Acta* **2001**, *1507*, 161−179.
(28) Sétif, P.; Fischer, N.; Lagoutte, B.; Bottin, H.; Rochaix, J.-D. *Biochim. Biophys. Acta* **2002**, *1555*, 204−209.
(29) Sétif, P. Q. Y.; Bottin, H. *Biochemistry* **1994**, *33*, 8495−8504.
(30) Sétif, P. Q. Y.; Bottin, H. *Biochemistry* **1995**, *34*, 9059−9070.
(31) Zehnder, A.; Wuhrmann, K. *Science* **1976**, *194*, 1165−1166.
(32) Rögner, M.; Nixon, P.; Diner, B. *J. Biol. Chem.* **1990**, *265*, 6189−6196.
(33) van Thor, J.; Geerlings, T.; Matthijs, H.; Hellingwerf, K. *Biochemistry* **1999**, *38*, 12735−12746.
(34) Palma, P. N.; Lagoutte, B.; Krippahl, L.; Moura, J. J. G.; Guerlesquin, F. *FEBS Lett.* **2005**, *579*, 4585−4590.

chromatographies.[34] Concentrations of Fd and FNR were measured spectrophotometrically at 422 and 460 nm using extinction coefficients of 9.7 and 10.5 $mM^{-1}\cdot cm^{-1}$, respectively.

Electrode Preparation. Surface-modified gold foils were used as working electrodes.[3] Gold foils (thickness between 1.5 and 2 μm) were made by vapor deposition (Edwards model 306) onto thoroughly cleaned glass slides. Slides were cleaned by a 30 min sonication in chloroform followed by thorough rinsing with water, a 30 min sonication in detergent, rinsing with water, a 30 min bath in a freshly prepared piranha solution[35] (1 volume 30% hydrogen peroxide, 2 volumes sulfuric acid), and rinsed extensively with water. The slides were dried under an argon or nitrogen flux and stored in a desiccator under vacuum until use.

For preparation of working electrodes, a gold foil was glued onto the tip of a glass tube (3 mm in diameter, surface area $S = 0.07$ cm^2) in which a stainless steel rod was mounted. Two glues were used, a standard epoxy resin for mechanical resistance and silver glue for electrical conductivity.

Before use, the electrodes were cleaned by immersion for 10 seconds in a freshly made sulfochromic acid solution (5% saturated $K_2Cr_2O_7$ solution in water, 95% sulfuric acid). Electrodes were tested and incubated in a 10 mM solution of 3-mercapto-1-propanol in ethanol for 90 min to allow for self-assembly of a hydroxyl-terminated monolayer at the surface. Finally, the modified electrodes were rinsed with ethanol then with water and stored in "partial" buffer before use to prevent the electrode from drying, as it was found that electrochemistry of cyt c_6 degrades when the electrode dries. Electrochemical tests ascertained that, at the potential range used in this work, only cytochrome c_6 is able to react with the electrode.

Electrochemical Measurements. A Parstat 2263 potentiostat controlled by a computer and PowerSuite software (Princeton Applied Research, Ametek, Trappes, France) was used for cyclic voltammetry. Data were extracted from the databases with the help of the mdbtools software (http://mdbtools.sourceforge.net/). Voltammograms displayed in this paper have negative anodic current. Unless otherwise stated potentials are given with respect to the saturated KCl calomel electrode (SCE).

The electrochemical cell contained three electrodes: a platinum wire counter electrode, a KCl saturated calomel reference electrode (SCE), and the gold working electrode described above. The working electrode was mounted into a microcell consisting of a glass tube closed at the bottom with a standard dialysis membrane (MW cutoff: 8kDa). This allowed working with a fairly low sample volume (usually 75 μL) while keeping good electrical conductivity.

Additions to the sample solution were made through a hole on the side of the glass microcell, with long pipet tips. Tips were plunging into the sample solution. An electrochemical calibration of the additions performed with ferricyanide showed that precision was better than 2% for successive additions of 1 μL.

To prevent oxygen from interfering with the measurements, the electrochemical cell was kept within an O_2-free glove box (usual concentration: 5 ppm O_2). All measurements were performed at 20 °C.

Experiments in dark conditions were recorded in weak ambient light, as no difference was found with a cell covered by a black cloth over a wide range of experimental conditions. Light conditions were obtained by illuminating the working electrode from the bottom with a halogen projector lamp. A Calflex IR filter (cutoff around 750 nm) was applied to prevent heating of the sample along with a long-pass red glass filter (cutoff around 600 nm) to prevent UV light from damaging FNR.

Optical Measurements. The dissociation constant between FNR and oxidized ferredoxin was measured by flash spectroscopy as described in ref 36. In the "partial" buffer, a value of 140 μM was obtained.

(35) Be careful, piranha solution reacts violently with organic compounds.
(36) Cassan, N.; Lagoutte, B.; Sétif, P. *J. Biol. Chem.* **2005**, *280*, 25960−25972.

As cytochrome c_6 has a potential much higher than that of ferredoxin, the reduction of oxidized cytochrome by reduced ferredoxin is thermodynamically favorable. This reaction would represent a short-circuit for the electron flow in our system.[37] Direct measurements of the rate constant of reduction of oxidized cytochrome c_6 by reduced ferredoxin were not practical because of the experimental difficulty in reducing the ferredoxin and separating it from the reductor while keeping it reduced. Rather, an anaerobic spectrometric cell containing 3 μM reduced cyt c_6, 3 μM oxidized Fd, and 0.3 μM photosystem I was subjected to cycles of illumination/darkness. Absorbance of the sample was measured at 553 nm.[38] Upon illumination, electrons are transferred from cyt c_6 to Fd via PSI. The photoreduced ferredoxin then reacts with oxidized cyt c_6. An equilibrium is rapidly reached. When the light is switched off, the forward electron-transfer ceases and the only reaction occurring in the cell is

$$c_6^{ox} + Fd_{red} \xrightarrow{k_{short}} c_6^{red} + Fd_{ox} \quad (1)$$

As originally all cyt c_6 is reduced, all Fd oxidized, and there is no other electron acceptor, at all times $[c_6^{ox}] = [Fd_{red}]$. We therefore expect second-order kinetics. Fits of the kinetics yield $k_{short} = 4 \pm 1 \times 10^6$ $M^{-1}\cdot s^{-1}$. The absence of interfering redox compounds was ascertained by the fact that successive traces superimpose perfectly.

This experiment also offers an alternative way to determine the rate constant k_{short}. If we assume that the forward electron transfer is limited by the second-order reaction between cyt c_6 and PSI (this is likely as electrochemical experiments show that this is the case even for much higher concentrations of cyt c_6), the consumption rate of reduced cyt c_6 is

$$v_- = k_3[c_6^{red}][PSI] \quad (2)$$

where $k_3 = 6 \times 10^6$ $M^{-1}\cdot s^{-1}$ is the second-order rate constant of reaction between cyt c_6 and PSI, following the notations in ref 3. The rate of its regeneration is given by

$$v_+ = k_{short}[c_6^{ox}][Fd_{red}] \quad (3)$$

When the equilibrium is reached, both rates are equal, and we can express k_{short}:

$$k_{short} = k_3 \frac{[c_6^{red}][PSI]}{[c_6^{ox}][Fd_{red}]} \quad (4)$$

One finds $k_{short} = 5 \pm 1 \times 10^6$ $M^{-1}\cdot s^{-1}$. Both methods are in good agreement and a value of $k_{short} = 5 \times 10^6$ $M^{-1}\cdot s^{-1}$ was used in the simulations below as it yielded the best fits (see figure S1 in Supporting Information).

Results and Discussion

Construction of the Electron-Transfer Chain. In a previous report, the interaction between cytochrome c_6 and photosystem I was investigated, using methylviologen (MV) as artificial electron acceptor for PSI.[3] In this configuration, MV was reoxidized by dissolved oxygen. These experiments allowed the determination of the rate constant of the reaction of cytochrome c_6 with PSI under steady-state conditions.[3] As the next step in the construction of a complete electron-transfer chain, we replaced MV with the natural acceptor of PSI, ferredoxin. First,

(37) In vivo, this problem does not arise as cyt c_6 and ferredoxin are separated by the thylakoid membrane.
(38) At 553 nm, we measured $\Delta\epsilon(c_6^{ox}/c_6^{red}) = 17850$ $M^{-1}\cdot cm^{-1}$ by oxydizing reduced cyt c_6 in a spectrometric cell with ferricyanide and $\Delta\epsilon(Fd_{red}/Fd_{ox}) = 2200$ $M^{-1}\cdot cm^{-1}$ by reducing ferredoxin with titane citrate and allowing it to be reoxidized by oxygen in a spectrometric cell.

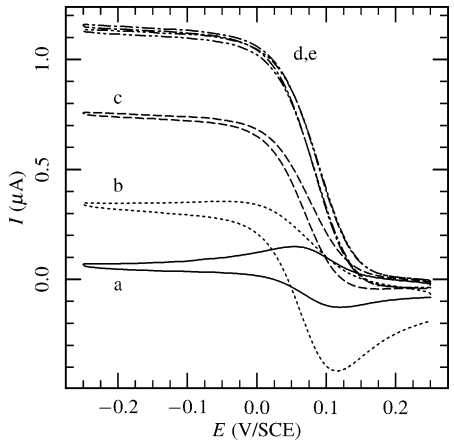

Figure 1. Cyclic voltammograms of cyt c_6 recorded in the dark (a) and under illumination (b−e): $[c_6] = 80\ \mu$M, [PSI] = 0.6 μM, [Fd] = 10 μM, [FNR] = 10 μM in the "complete" buffer. The amount of GLDH was varied: 0 U (b), 1.5 U (c), 7.5 U (d), and 9 U (e). No background substraction was performed.

measurements were conducted as follows: In a deaerated solution containing oxidized cyt c_6, PSI and oxidized ferredoxin, cyclic voltammograms were recorded both in dark and light conditions, from 0.25 to −0.25 V versus SCE. During the sweep, reduced cyt c_6 is formed at the electrode. In dark conditions, no chemical reaction takes place, and the voltammograms recorded were identical to those obtained in the absence of PSI and Fd. However, upon illumination, PSI catalyzes the transfer of electrons from cyt c_6 to Fd. The expected photocatalytic process taking place under illumination is therefore

$$c_6^{ox} + e^- \overset{\text{electrode}}{\rightleftharpoons} c_6^{red} \quad (5)$$

$$c_6^{red} + Fd_{ox} \xrightarrow[\text{light}]{\text{PSI}} Fd_{red} + c_6^{ox} \quad (6)$$

However, unlike what was observed with MV, the voltammograms obtained under illumination, even in the presence of an excess of Fd, differ only very slightly from those in dark condition, meaning that photocatalysis is weak (figure S5 in Supporting Information). This can be accounted for by the very favorable oxidation of reduced Fd by cyt c_6 (reaction 7)[39] which, by consuming c_6^{ox}, decreases the catalytic current.

$$c_6^{ox} + Fd_{red} \xrightarrow[k_{short}]{\Delta E > 700\ \text{mV}} c_6^{red} + Fd_{ox} \quad (7)$$

To improve catalysis, we introduced FNR as a partner of ferredoxin that would regenerate oxidized ferredoxin. FNR catalyzes reduction of $NADP^+$ to NADPH by ferredoxin (reaction 8) and has been studied rather extensively.[4,7,40−42] Cyclic voltammograms were recorded in both dark and light conditions in the presence of FNR and $NADP^+$; they are represented in Figure 1(traces a and b). Under light conditions, the following reaction occurs in addition to reactions 5 and 6:

$$2Fd_{red} + NADP^+ + H^+ \xrightarrow{\text{FNR}} 2Fd_{ox} + NADPH \quad (8)$$

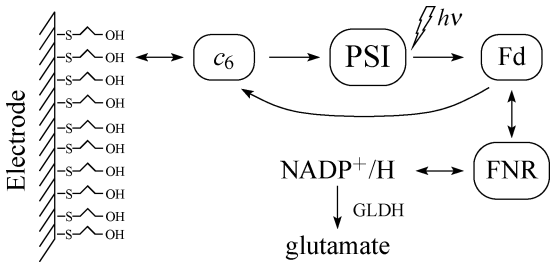

Figure 2. Electron-transfer chain under illumination. Single arrows represent irreversible electron transfers whereas double arrows represent reversible electron transfers. The mechanism of electron transfer involving FNR was simplified for the sake of clarity.

As can be seen in Figure 1b, in the presence of FNR the forward (cathodic) trace of the voltammogram increases in intensity while developing a characteristic sigmoidal shape. This indicates that the global photocatalytic process depicted above now becomes more efficient. The occurrence of a plateau current, even when ferredoxin is introduced at a lower concentration than cyt c_6, shows that there is no diffusional limitation to catalysis, as a result of the efficient regeneration of Fd_{ox} by the FNR-catalyzed cycle.

However, voltammograms recorded under illumination also display a large, intense reoxidation peak evidencing that some catalytic process involving a diffusing species is taking place during the backward scan of the voltammogram. This observation can be explained by the fact that FNR is a reversible enzyme meaning that it can also function as a diaphorase,[41] reducing ferredoxin in the presence of NADPH. Considering the concomitant occurrence of the short circuit reaction 7, the overall catalytic cycle taking place at the electrode during the anodic scan is therefore

$$c_6^{red} \overset{\text{electrode}}{\rightleftharpoons} c_6^{ox} + e^- \quad (9)$$

$$NADPH + 2c_6^{ox} \xrightarrow{\text{FNR, Fd}} NADP^+ + H^+ + 2c_6^{red} \quad (10)$$

In the cathodic scan, when cyt c_6 is reduced at the electrode, reaction 10 has the sole effect of reducing the net cathodic catalytic current.

To minimize the undesirable short-circuit, it is necessary to recycle efficiently NADPH back to $NADP^+$ to keep the NAPDH concentration very low. We used GLDH to achieve this. GLDH catalyzes the conversion of α-ketoglutarate (α-KG) to glutamate linked to the oxidation of NADPH:[43]

$$\alpha\text{-KG} + NH_4^+ + NADPH \rightarrow \text{glutamate} + NADP^+ \quad (11)$$

At the pH and the concentrations used, this reaction is complete. When the concentration of GLDH and its substrates are high enough, the concentration of NADPH is kept at negligible levels thereby suppressing reaction 10. Dark and light cyclic voltammograms obtained in the presence of cyt c_6, PSI, Fd, FNR, $NADP^+$, GLDH, α-KG, and ammonium are shown in Figure 1 (traces c to e). It can be clearly seen that, as the GLDH concentration increases, the return peak diminishes while the plateau current increases. A saturation is obtained for around nine units of GLDH for 75 μL of sample (trace e). Under these conditions the voltammograms recorded upon illumination

(39) The potential of the couple c_6^{ox}/c_6^{red} is 321 mV (vs NHE) whereas the one of Fd_{ox}/Fd_{red} is around −420 mV vs NHE[4].
(40) Batie, C.; Kamin, H. *J. Biol. Chem.* **1981**, *256*, 7756−7763.
(41) Batie, C.; Kamin, H. *J. Biol. Chem.* **1984**, *259*, 11976−11985.
(42) Batie, C.; Kamin, H. *J. Biol. Chem.* **1984**, *259*, 8832−8839.
(43) Shimizu, H.; Kuratsu, T.; Hirata, F. *J. Ferment. Technol.* **1979**, *57*, 428−433.

display a perfect catalytic shape, without hysteresis, demonstrating that the recycling is satisfying. Nine units of GLDH were therefore used in all other experiments.

The complete electron-transfer chain is represented in Figure 2.

Functional Model Used for PSI Interactions. The PSI-catalyzed light-induced electron transfer from reduced cyt c_6 (c_6^{red}) toward oxidized ferredoxin (Fd_{ox}) was kinetically modeled as follows. The proposed simplified model is reduced to the minimum number of *functional* kinetic equations representing the steady-state attained upon illumination:

$$c_6^{ox} + e^- \overset{\text{electrode}}{\rightleftharpoons} c_6^{red} \tag{12}$$

$$(P700, F_{AB}) \xrightarrow[\text{fast}]{\text{light}} (P700^+, F_{AB}^-) \tag{13}$$

$$c_6^{red} + (P700^+, F_{AB}^-) \xrightarrow{k_3} c_6^{ox} + (P700, F_{AB}^-) \tag{14}$$

$$(P700, F_{AB}^-) + Fd_{ox} \xrightarrow{k_{on}} (P700, F_{AB}^-)Fd_{ox} \tag{15}$$

$$(P700, F_{AB}^-)Fd_{ox} \xrightarrow{\text{fast}} (P700, F_{AB})Fd_{red} \tag{16}$$

$$(P700, F_{AB})Fd_{red} \xrightarrow{k_{off}} (P700, F_{AB}) + Fd_{red} \tag{17}$$

$(P700, F_{AB})$, $(P700^+, F_{AB}^-)$, and $(P700, F_{AB}^-)$ represent respectively the PSI reaction center in the ground-state, after charge separation, and after reduction of $P700^+$. $(P700^+, F^-{}_{AB})$ is assumed to first react with cyt c_6 rather than Fd_{ox} since cyt c_6 is introduced in excess with respect to Fd.

The following simplifying assumptions are made:

(i) Light absorption by PSI and ensuing charge separation are assumed to be fast. This was experimentally ascertained by working under saturating illumination conditions for which the catalytic current was independent of the actinic light intensity.

(ii) Charge recombination, being a slow process ($\approx$ 80 ms) compared to further reactions of $(P700^+, F_{AB}^-)$,[2] was ignored.

(iii) The electron transfer between c_6^{red} and $(P700^+, F_{AB}^-)$ is purely collisional as demonstrated previously.[3,44]

(iv) Formation of the $(P700, F_{AB}^-)Fd_{ox}$ complex, characterized by a rate constant k_{on}, is assumed to be irreversible since it is followed by rapid internal electron transfer: dissociation of the $(P700, F_{AB}^-)Fd_{ox}$ complex is expected to occur in the ms time range,[36] whereas the electron-transfer step is characterized by μs kinetics.[29]

(v) The internal electron transfer between $(P700, F_{AB}^-)$ and Fd_{ox}, taking place within the $(P700, F_{AB}^-)Fd_{ox}$ complex, is considered as being irreversible owing to its high exergonicity and fast dissociation.

(vi) Dissociation of the $(P700,F_{AB})Fd_{red}$ complex, characterized by the rate constant k_{off}, is assumed to be irreversible. This is justified since this dissociation is followed by fast consumption of the highly reducing species Fd_{red} by the recycling reaction.

Considering the very low concentration of PSI involved here it is legitimate to apply the steady state approximation to PSI in each of its redox states, which yields the following expression for the rate of the PSI-catalyzed electron transfer between c_6^{red} and Fd_{ox} (derivation available in Supporting Information):

$$V_{cat} = \frac{k_3[c_6^{red}]\, C_{PSI}^0}{1 + k_3\,[c_6^{red}]\left(\dfrac{1}{k_{off}} + \dfrac{1}{k_{on}\,[Fd_{ox}]}\right)} \tag{18}$$

with C_{PSI}^0 the bulk concentration of photosystem I. In the most general case $[Fd_{ox}]$ and $[c_6^{red}]$ are functions of time and distance away from the electrode surface.

Kinetic Analysis of the cyt c_6/PSI/Fd Electron-Transfer Chain: Total Recycling Assumption. We now specifically consider the limiting situation, further referred to as the total recycling condition, where recycling of Fd to its oxidized state by the FNR cycle (see above) is fast enough to ensure that $[Fd_{ox}] = C_{Fd}^0$, with C_{Fd}^0 the bulk concentration of ferredoxin. As previously shown[3,13] an analytical expression for the catalytic plateau current, i_{cat} can then be obtained by solving the following set of differential equations, consisting of the 2nd Ficks law and the relation between the current, i, and the c_6^{red} concentration:

$$\begin{cases} \dfrac{\partial\,[c_6^{red}]}{\partial t} = D\,\dfrac{\partial^2[c_6^{red}]}{\partial x^2} - \dfrac{k_3\,[c_6^{red}]\,C_{PSI}^0}{1 + k_3\,[c_6^{red}]\left(\dfrac{1}{k_{off}} + \dfrac{1}{k_{on}C_{Fd}^0}\right)} = 0 \\ i = -FSD\left(\dfrac{\partial[c_6^{red}]}{\partial x}\right)_{x=0} \end{cases} \tag{19}$$

where D is the diffusion coefficient of cyt c_6, t is the time variable, x is the distance from the electrode, F is the Faraday constant, and S is the electrode surface area. With the boundary conditions: $x = 0$: $[c_6^{red}] = C_6^0$, $x = +\infty$: $[c_6^{red}] = 0$, where C_6^0 is the bulk cyt c_6 concentration, one obtains

$$i_{cat} = FSC_6^0\sqrt{k_{app}C_{PSI}^0 D} \tag{20}$$

k_{app} is an apparent second-order rate constant, related to the values of the individual kinetic constants of the above mechanism by

$$k_{app} = k_3 \times \frac{2}{\sigma}\left\{1 - \frac{1}{\sigma}\ln(1+\sigma)\right\} \tag{21}$$

with σ a dimensionless parameter characterizing the ratio of the reduction and the oxidation rates of PSI, given by

$$\sigma = k_3 C_6^0\left(\frac{1}{k_{off}} + \frac{1}{k_{on}C_{Fd}^0}\right) \tag{22}$$

The above expression of σ suggests the experimental strategy followed below to determine the individual values of k_3, k_{off}, and k_{on}. Experimentally it is convenient to use as an observable the catalytic efficiency, defined as the ratio of i_{cat} over the current recorded in the dark, i_{dark}:

$$\frac{i_{cat}}{i_{dark}} = 2.24\sqrt{RTC_{PSI}^0 k_{app}/F\upsilon} \tag{23}$$

υ being the potential scan rate.

Determination of k_3. Decreasing C_6^0 sufficiently allows us to reach a limiting situation corresponding to $\sigma \ll 1$, for which $k_{app} = k_3$. This pseudo first-order situation corresponds to the reduction of PSI by cyt c_6 being the rate-determining step of the system. The attainment of this situation can be experimen-

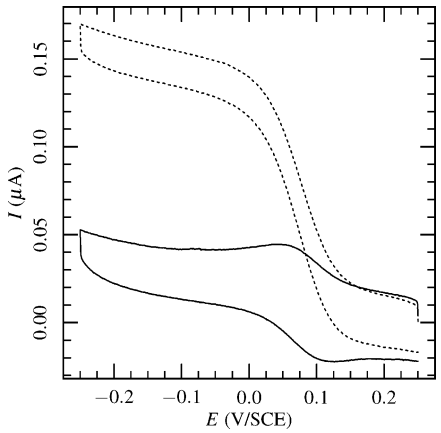

Figure 3. Photoinduced PSI-catalyzed reduction of ferredoxin by cyt c_6. Cyclic voltammograms recorded at low cyt c_6 concentration (15 μM) in the dark (solid line) or under saturating illumination (dotted line). Scan rate ν = 10 mV/s. The deaerated solution contained PSI = 0.4 μM, ferredoxin = 3 μM, FNR = 3 μM, GLDH = 9 units, in the "complete" buffer.

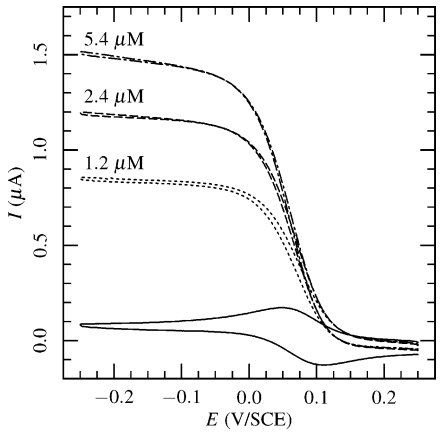

Figure 4. Photoinduced PSI-catalyzed reduction of ferredoxin by cyt c_6. Cyclic voltammograms recorded at high cyt c_6 concentration (100 μM), in the dark (solid line) or under saturating illumination (dotted lines), for the ferredoxin concentrations indicated on each curve. Scan rate ν = 6 mV/s. The deaerated solution contained PSI = 1.3 μM, FNR = 16 μM, GLDH = 9 units, in the "complete" buffer. The background was not substracted.

tally ascertained by observing that, as predicted by the above equations, the catalytic efficiency no longer depends on C_6^0. We observed that such was the case for $C_6^0 \approx$ <15 μM, and from the intense catalytic signal thus obtained (see Figure 3) we derived a value of $k_3 = 6 \pm 1 \times 10^6$ $M^{-1}\cdot s^{-1}$ using eq 23. This later value is in agreement both with the value we determined earlier for a slightly different system[3] and with the value of 5.9×10^6 $M^{-1}\cdot s^{-1}$ measured for the present system by laser-flash experiments.[44]

Determination of k_{on} and k_{off}. Once k_3 is known, one can go back to the general case situation by increasing the cyt c_6 concentration, so that the reactions between PSI and Fd now contribute to the observed overall kinetics. To this aim C_6^0 was fixed at 100 μM and the Fd concentration systematically varied from $\sim$ 1 to 20 μM. A family of intense S-shaped catalytic voltammograms was then obtained, some of which are represented in Figure 4.

The corresponding catalytic efficiencies were measured for each ferredoxin concentration and are plotted as a function of C_{Fd}^0 in Figure 5 (triangles). As can be seen, the catalytic

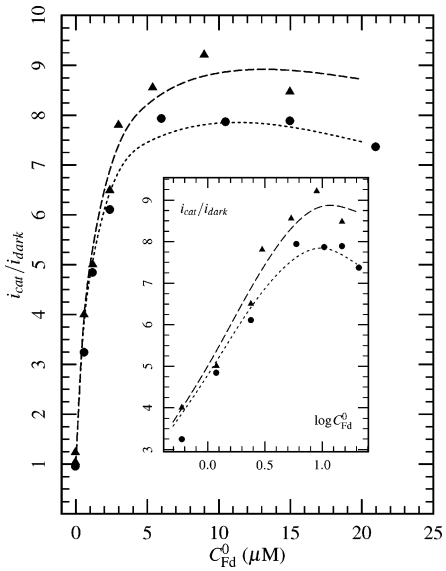

Figure 5. Variation of the catalytic efficiency, i_{cat}/i_{dark}, recorded at C_6^0 = 100 μM, as a function of the ferredoxin concentration for C_{FNR}^0 = 16 μM (▲) and C_{FNR}^0 = 8 μM (●). Scan rate ν = 6 mV/s. The deaerated solution contained PSI = 1.3 μM and GLDH = 9 units in the "complete" buffer. Lines are simulated catalytic efficiencies.

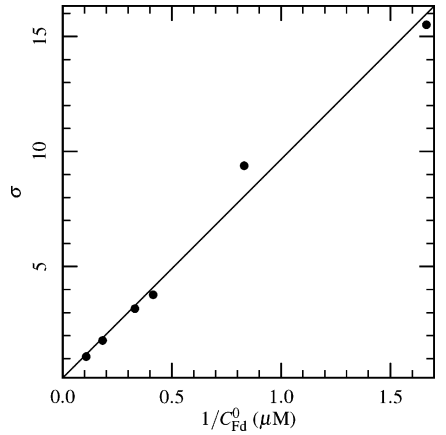

Figure 6. Variation of the parameter σ derived form the measurement of the catalytic efficiency recorded for C_6^0 = 100 μM, C_{FNR}^0 = 16 μM, and for various ferredoxin concentrations C_{Fd}^0, as a function of $1/C_{Fd}^0$.

efficiency first increases rapidly with increasing C_{Fd}^0 and then tends to level-off for C_{Fd}^0 > 5 μM. Using eqs 23 and 21 the global parameter σ was derived from the value of the catalytic efficiency for each ferredoxin concentration, and, as suggested by eq 22, σ was plotted as function of $1/C_{Fd}^0$. As can be seen in Figure 6, a straight line is obtained as expected. From the origin of this line a value of $k_{off} = 3200 \pm 500$ s^{-1} is derived while, from its slope, a value of $k_{on} = 7 \pm 1 \times 10^7$ $M^{-1}\cdot s^{-1}$ is determined. The k_{off} value is in agreement with the lower limit of 800 s^{-1} obtained by flash spectroscopy.[36] However the value derived here for k_{on} is clearly underestimated since values as high as 3.5×10^8 $M^{-1}\cdot s^{-1}$ were reported for this rate constant.[27] This apparent discrepancy probably finds its origin in the failure of the recycling FNR/Fd reaction which cannot maintain the condition $[Fd_{ox}] = C_{Fd}^0$. The actual Fd_{ox} concentration in the electrode vicinity then results from a balance of the PSI-

(44) Hervás, M.; Navarro, J. A.; Díaz, A.; Bottin, H.; la Rosa, M. A. D. *Biochemistry* **1995**, *34*, 11321−11326.

catalyzed electron transfer, the cyt c_6^{ox}/Fd_{red} short-circuit, and the FNR-catalyzed recycling reaction.

Kinetic Analysis of the cyt c6/PSI/Fd Electron-Transfer Chain: Coupling to the FNR/Fd Electron Transfer. To evidence the interfering role of the kinetics of the Fd/FNR recycling reaction, the FNR concentration was lowered from 16 to 8 μM. The catalytic efficiency was then measured under these conditions and plotted as a function of the ferredoxin concentration (Figure 5, dots). As can be seen the catalytic efficiency recorded at low Fd concentration was unaffected by a decrease of the FNR concentration. However for [Fd] > 5 μM the catalytic efficiency is not only lower than the one recorded for $C^0_{FNR} = 16\ \mu$M but also decreases with increasing ferredoxin concentration. This dependence of the catalytic efficiency on the FNR concentration demonstrates that the FNR-catalyzed recycling of Fd_{ox} is not fast enough to ensure fulfillment of the total recycling condition. As a result not only $[Fd_{ox}] < C^0_{Fd}$ but the short circuit reaction between Fd_{red} and c_6^{ox} then probably competes with the FNR-catalyzed recycling reaction, thus also decreasing the catalysis. Moreover, the very fact that, for $C^0_{FNR} = 8\ \mu$M, a decrease of the catalytic efficiency is observed for increasing Fd concentration points to an unexpected inhibiting effect of Fd_{ox}, occurring at a yet unidentified stage of the overall catalytic process (but see later).

The aforementioned results evidence that the catalytic response of the system is jointly controlled by the cyt c_6/PSI/Fd electron-transport chain and the coupled FNR/Fd electron-transfer reaction. Analysis of cyclic voltammetry data can therefore bring information about both the PSI and the FNR-catalyzed electron transfers, provided the influence of these reactions on the measured catalytic signal can be deciphered. This requires that a detailed kinetic mechanism is proposed for the FNR-catalyzed Fd_{ox} regeneration.

Proposed Functional Mechanism for the FNR-Catalyzed Regeneration of Fd_{ox}. The following mechanism is used to model the kinetics of the FNR-catalyzed regeneration of Fd_{ox}. It describes the successive transfer of two electrons involving two Fd_{red} molecules to the FNR-$NADP^+$ complex. It is similar to the mechanism proposed in Figure 2 of ref 7. The FNR species in bold characters are FNR-$NADP^+$ complexes.

$$\left.\begin{array}{ll}\textbf{(I)} & Fd_{red} + \mathbf{FNR_{ox}} \overset{K_d^I = 140\ \mu M}{\rightleftharpoons} \mathbf{Fd_{red}FNR_{ox}} \\ \textbf{(II)} & \mathbf{Fd_{red}FNR_{ox}} \xrightarrow{k_{ET1} = 6200\ s^{-1}} \mathbf{FNR_{sq}Fd_{ox}} \\ \textbf{(III)} & \mathbf{FNR_{sq}Fd_{ox}} \overset{K_d^{II} = 3\ \mu M}{\rightleftharpoons} Fd_{ox} + \mathbf{FNR_{sq}}\end{array}\right| 1e^-$$

$$\left.\begin{array}{ll}\textbf{(IV)} & Fd_{red} + \mathbf{FNR_{sq}} \overset{K_d^{IV} = 140\ \mu M}{\rightleftharpoons} \mathbf{Fd_{red}FNR_{sq}} \\ \textbf{(V)} & \mathbf{Fd_{red}FNR_{sq}} \xrightarrow{k_{ET2} = 6200\ s^{-1}} \mathbf{FNR_{red}Fd_{ox}} \\ \textbf{(VI)} & \mathbf{FNR_{red}Fd_{ox}} \xrightarrow[irrev.]{fast} Fd_{ox} + \mathbf{FNR_{red}}\end{array}\right| 1e^-$$

$$\mathbf{FNR_{red}} \xrightarrow[irrev.]{fast} FNR + NADPH$$

$$FNR + NADP^+ \xrightarrow[irrev.]{fast} \mathbf{FNR_{ox}}$$

Two Fd_{red} molecules are assumed to successively dock to the FNR-$NADP^+$ complex (**FNR**). The first Fd_{red} molecule reduces the FAD prosthetic group of FNR to its semiquinone form (**FNR_{sq}**) and the second to its fully reduced state (**FNR_{red}**). Fd_{ox} is released reversibly after each reduction step. The value of 6200 s^{-1} taken for the rate constant of the electron-transfer steps II and V is derived from literature.[33] Reduction of $NADP^+$ within the FNR_{red}-$NADP^+$ complex (**FNR_{red}**) is assumed to be both irreversible (since NADPH is rapidly replaced by $NADP^+$ present in a very large millimolar excess), and fast, in accordance with the known fast kinetics of $NADP^+$ reduction by reduced FNR.[41,45] For the same reason formation of the FNR_{ox}-$NADP^+$ complex (**FNR_{ox}**) is assumed to be rapid. The "reverse", diaphorase-like, functioning of FNR, which consists in catalyzing the oxidation of NADPH by Fd_{ox}, is assumed to be totally prevented by the presence of the NADPH-consuming GLDH catalytic cycle, optimized as described in the section Construction of the Electron-Transfer Chain. Considering the difficulty in treating analytically the coupling of the cyt c_6/PSI/Fd and the FNR/Fd electron-transfer chains, kinetic analysis was carried out on the basis of numerical simulations using the DIGISIM 2.0 software.[46] This program allows the complete sets of kinetic equations given above to be implemented and to calculate the resulting catalytic voltammogram, provided all the kinetic constants are known. At this stage however, the only known rate constants are that of the cyt c_6/Fd short circuit (k_{short}, determined in Experimental Section), k_3, and k_{off}, determined above.[47] To reduce the number of parameters involved we tried to evaluate the values of the dissociation constants for the FNR/Fd complexes independently from the voltammetric measurements. Three redox states are to be considered for FNR (ox, sq, and red) and two for Fd (ox and red) but, as seen from the above mechanism, only five dissociation constants are needed here corresponding to the following complexes: **$FNR_{ox}Fd_{ox}$, $FNR_{ox}Fd_{red}$, $FNR_{sq}Fd_{ox}$, $FNR_{sq}Fd_{red}$, $FNR_{red}Fd_{ox}$**.

Evaluation of the Dissociation Constant of the FNR/Fd Complexes. The only directly measurable dissociation constant is the one corresponding to the FNR_{ox}/Fd_{ox} complex:

$$Fd_{ox} + FNR_{ox} \overset{K_d}{\rightleftharpoons} FNR_{ox}Fd_{ox} \qquad (24)$$

Proceeding as indicated in the Experimental Section, we measured for this constant a value of $K_d = 140\ \mu$M for the intermediate form of FNR. This value, though rather high, can be easily explained: according to ref 40, Figure 1, a value around 40 μM should be expected for the short form of FNR with the given ionic strength. As Cassan et al.[36] reported that dissociation constants with the intermediate form are consistently three to four times higher than the ones for the short form, a value of 120−150 μM seems reasonable for the intermediate form in the conditions we used.

Since C^0_{Fd} and C^0_{FNR} used here are both much lower than 140 μM, one can conclude that complexation of Fd_{ox} by FNR_{ox} is only occurring to a small extent. This result excludes depletion

(45) Tejero, J.; Peregrina, J. R.; Martinez-Julvez, M.; Gutierrez, A.; Gomez-Moreno, C.; Scrutton, N. S.; Medina, M. *Arch. Biochem. Biophys.* **2007**, *459*, 79−90.
(46) DigiSim software from Bioanalytical Systems Inc. (West Lafayette, IN).
(47) The values of the diffusion coefficients of all the species are also needed. We previously determined the diffusion coefficient of cyt c_6: $D = 1.2 \times 10^{-6}$ cm^2/s.[3] From the respective sizes of cyt c_6 (~2 nm in diameter), Fd (2 nm), FNR (4.5 nm), and PSI (≈ 8 nm), the diffusion coefficients of these three later species were taken respectively as 10^{-6}, 5×10^{-7}, and 10^{-7} cm^2/s. The calculated catalytic efficiency was found to depend only very weakly on the exact values taken for the diffusion coefficients.

of Fd_{ox} by favorable formation of the $FNR_{ox}Fd_{ox}$ complex as the origin of the observed decay of catalysis with increasing C^0_{Fd}.

It must be noted that the measured K_d is not directly the one of interest for the reactions, as measurements were done in the absence of $NADP^+$.[48] However, no significant differences were found with experiments on the short form of FNR with or without $NADP^+$; it is expected to be the same for the intermediate form.

As no simple method exists to determine directly dissociation constants of reactions I, III, and IV, a simple heuristic has been used to provide starting values for the simulations. These values were confirmed by the consistency of the simulated catalytic values with the measured ones. A first step was to take all the K^j_d equal to K_d, neglecting the redox state of the proteins. However, this set of parameters failed to reproduce the decrease of the catalytic efficiency at high ferredoxin concentrations seen in Figure 5 for $C^0_{FNR} = 8\ \mu M$ (circles).

A deeper analysis shows that this set of values is not consistent with the findings of Batie and Kamin[40] and Pueyo et al.[49] that the potential of ferredoxin shifts 50−100 mV toward more negative values whithin the FNR/ferredoxin complex. Let us consider the following thermodynamic cycle for the reactions I and III:

$$\begin{array}{ccc} Fd_{red} + \mathbf{FNR_{ox}} & \xleftrightarrow{K_d^{I}} & \mathbf{Fd_{red}FNR_{ox}} \\ \Big\updownarrow K_{ext} & & \Big\updownarrow K_{int} \\ Fd_{ox} + \mathbf{FNR_{sq}} & \xleftrightarrow{K_d^{III}} & \mathbf{Fd_{ox}FNR_{sq}} \end{array}$$

The equilibrium constants K_{ext} and K_{int} are linked to the difference of potential between the Fd_{ox}/Fd_{red} and the FNR_{ox}/FNR_{sq} couples respectively outside (ΔE_{ext}) and whithin (ΔE_{int}) the complex by the relation

$$K_i = \exp\left\{-\frac{F\Delta E_i}{RT}\right\} \tag{25}$$

From the equivalence of the pathways from one point to another in the thermodynamic cycle follows

$$K_{ext} \times K_d^{III} = K_d^{I} \times K_{int} \tag{26}$$

The reported shifts in potential imply that K_d^{III} must be 7 to 50 times smaller than K_d^{I}. This leads to the following values $K_d^{I} = 140\ \mu M$, $K_d^{III} = 3\ \mu M$, and $K_d^{IV} = 140\ \mu M$.

Simulation of the Catalytic Behavior of the PSI/FNR Coupled System. The only remaining unknown parameters are, as far as the FNR/Fd complexation is concerned, the "on" rate constants for the formation of the FNR-Fd complexes described in reactions I, III, IV. The corresponding "off" rate constants are simply given by: $k^j_{off} = k^j_{on}K^j_d$ with j = I, III, IV. It can be confidently assumed that the possible range for the k^j_{on} values is $10^7-10^9\ M^{-1}\cdot s^{-1}$ [36] with the lowest values corresponding to the reactions with the highest K^j_d. The other unknown is the value of k_{on} for the formation of the $(P700, F^-_{AB})/Fd_{ox}$ complex which is expected to lie in the $10^8-10^9\ M^{-1}\cdot s^{-1}$ range.[29]

Numerous simulations were ran choosing for k_{on} and k^j_{on} values within the above permitted ranges, from which the following conclusions were drawn. We observed that the exact k^j_{on} values given for the formation of the complexes $\mathbf{FNR_{ox}}$-$\mathbf{Fd_{red}}$, $\mathbf{FNR_{sq}Fd_{ox}}$, $\mathbf{FNR_{sq}Fd_{red}}$, and $\mathbf{FNR_{red}Fd_{ox}}$ had little effect on the value of the simulated plateau current (Figure S2 in Supporting Information). This result indicates that formation of the $\mathbf{FNR_{ox}Fd_{red}}$, $\mathbf{FNR_{sq}Fd_{ox}}$, and $\mathbf{FNR_{sq}Fd_{red}}$ complexes can be considered as being at equilibrium and that the kinetics of dissociation of the $\mathbf{FNR_{red}Fd_{ox}}$ complex does not participate in the kinetic control of the FNR-catalyzed recycling reaction. As a result reactions I, III, IV are only characterized by their respective K^j_d values estimated above.

Now that we have a reasonable set of values for the kinetic model, the catalytic behavior of the complete system can be simulated. In particular the variation of the catalytic efficiency with the ferredoxin concentration can be calculated and adjusted to the experimental variation using k_{on}, the rate constant for the formation of the $(P700, F^-_{AB})/Fd_{ox}$ complex, as a *single* adjustable parameter. As seen in Figure 5, a good agreement between the theoretical and experimental variations is observed for a value of $k_{on} = 2 \times 10^8\ M^{-1}\cdot s^{-1}$ which is consistent with the values around $3.5 \times 10^8\ M^{-1}\cdot s^{-1}$ obtained by laser-flash experiments.[27,36] But the most satisfying result is that the simulations also allow a reproduction of the decrease of catalytic efficiency with increasing Fd concentration consistently observed for $C^0_{FNR} = 8\ \mu M$ (see Figure 5). Insights into the origin of this unexpected behavior can be gained by analyzing the effect of small variations of the kinetic and thermodynamic parameters used so far in the simulations. In particular, the value given to K_d^{III} (dissociation constant of the $\mathbf{FNR_{sq}Fd_{ox}}$ complex) is observed to have a large effect on the simulated catalysis, the peak-shaped variation of the calculated catalytic efficiency with C^0_{Fd}, even disappearing if a value higher than 6 μM is assigned to K_d^{III}.[50] This result allows an unambiguous identification the origin of the inhibiting effect of Fd_{ox}: increasing the Fd_{ox} concentration impedes the already thermodynamically unfavorable dissociation of the $\mathbf{FNR_{sq}Fd_{ox}}$ complex (reaction III) thereby slowing significantly the FNR-catalyzed Fd_{ox} regeneration cycle. In other words increasing C^0_{Fd} above ~5 μM results in trapping FNR in its semiquinone form (FNR_{sq}). This unexpected inhibition of FNR kinetics by Fd_{ox} is particularly clearly evidenced in the here reported voltametric experiments since the resulting accumulation of Fd_{red} favors the c_6^{ox}-Fd_{red} short-circuit, which in turn induces a notable decrease of the catalytic efficiency.

A value of $K_d^{IV} \gg K_d^{III}$ is also required to reproduce the inhibiting effect of Fd_{ox}. This comes from the fact that, as seen from the above sequence of reactions, formation of the $\mathbf{FNR_{sq}}$-$\mathbf{Fd_{red}}$ complex competes with the formation of the inhibiting $\mathbf{FNR_{sq}Fd_{ox}}$ complex. The very fact that Fd_{ox}-dependent inhibition of the FNR cycle is experimentally observed is thus clear evidence that $K_d^{IV} \gg K_d^{III}$. More precisely a value of $K_d^{IV} > 70\ \mu M$ is required to reproduce the experimental value of catalytic efficiency within 10% (taking $K_d^{III} = 3\ \mu M$).[51]

(48) In the presence of $NADP^+$, the kinetic traces of the absorption evolution are more delicate to deconvolve, and the values obtained are much less precise.

(49) Pueyo, J.; Revilla, C.; Mayhew, S. G.; Gomez-Moreno, C. *Arch. Biochem. Biophys*. **1992**, *294*, 367−372.

(50) Typically a value in the range of $K_d^{III} = 2-6\ \mu M$ is required to reproduce the experimental catalytic efficiency with an accuracy better than 10% (see figure S3 in Supporting Information).

(51) See figure S4 in Supporting Information for more details.

Conclusion

The photodriven electron-transport chain from cyt c_6 to NADPH was fully reconstituted in solution and studied under stationary conditions by cyclic voltammetry. It is demonstrated herein that, provided a careful kinetic analysis is carried out, the experimental conditions can be finely tuned so that the characteristic rate and thermodynamic constants of several key steps of the electron-transport process can be quantified. Not only were the rate constants characterizing the cyt c_6/PSI and PSI/Fd electron transfers determined independently, but careful analysis of the variation of the catalytic efficiency with ferredoxin concentration revealed an unexpected inhibiting effect of Fd_{ox}. Based on simulations of the voltammetric signals and kinetic modeling of the FNR-catalyzed Fd oxidation, this effect was fully rationalized on the basis of the unfavorable dissociation of the $\mathbf{FNR_{sq}Fd_{ox}}$ complex.

Acknowledgment. We are grateful to Ms. Véronique Mary for expert technical assistance, to Dr. Alain Boussac for his generous gift of protein extracts, and to Dr. Vanessa Proux, Pr. Christian Bourdillon, and Dr. Hervé Bottin for their insightful discussions and suggestions. This work was supported by the European Union through the STRP network Solar-H, by ANR PhotobioH_2, and by the Biohydrogen program of DSV CEA.

Supporting Information Available: Derivation of all equations and supplementary data. This material is available free of charge via the Internet at http://pubs.acs.org.

JA0714787